ISSN 1063-7834, Physics of the Solid State, 2025, Vol. 67, No. 5, pp. 356–366. © Pleiades Publishing, Ltd., 2025.

Structural, Elastic, Mechanic, Electronic, and Thermodynamic of $LiMoN_2$ Compound for Electronic and Energy Storage

A. Djemli[a,b], M. Reffas[c], K. Bouferrache[c,d], F. Benlakhdar[e], R. Yekhlef[f,g], D. Belfennache[f,g], Sameh I. Ahmed[h,*], Z. Zerrougui[i], T. Chihi[c], M. A. Ghebouli[c,j], M. Fatmi[c,], and B. Ghebouli[i]**

[a] *Physics and Chemistry of Materials Lab, Department of Physics, University Mohamed Boudiaf of M'sila, M'sila, 28000 Algeria*

[b] *Faculty of Physics, University of Sciences and Technology Houari Boumediene (U.S.T.H.B), El Alia, BP 32, Bab Ezzouar, Algiers, 16111 Algeria*

[c] *Research Unit on Emerging Materials (RUEM), University Ferhat Abbas of Setif 1, Setif, 19000 Algeria*

[d] *Department of Physics, Faculty of Sciences, University of M'sila University Pole, Road Bourdj Bou Arreiridj, 28000 M'sila, Algeria*

[e] *Electronics Department, Faculty of Technology, University Ferhat Abbas of Setif 1, Setif, 19000 Algeria*

[f] *Research Center in Industrial Technologies CRTI, P.O. Box 64, Cheraga, Algiers, 16014 Algeria*

[g] *Laboratory of Electrochemistry, Molecular Engineering and Redox Catalysis (LEIMCR) Department of Engineering Process, Faculty of Technology, Ferhat Abbas University Setif-1, Setif, 19000 Algeria*

[h] *Department of Physics, College of Sciences, Taif University, P.O. Box 11099, Taif, 21944 Saudi Arabia*

[i] *Laboratory of Studies Surfaces and Interfaces of Solids Materials, Faculty of Technology, University Ferhat Abbas of Setif 1, Setif, 19000 Algeria*

[j] *Department of Chemistry, Faculty of Sciences, University of M'sila University Pole, Road Bourdj Bou Arreiridj, 28000 M'sila, Algeria*

**e-mail: fatmimessaoud@yahoo.fr*

*** e-mail: a.sameh@tu.edu.sa*

Received February 3, 2025; revised March 12, 2025; accepted March 12, 2025

Abstract—This study explores the structural, elastic, mechanical, electronic, and thermodynamic properties of the $LiMoN_2$ compound using ab initio calculations based on density functional theory (DFT). The compound's hexagonal structure exhibits intriguing characteristics, including metallic conductivity and strong Mo–N bonding. Elastic constants confirm its stability under pressures up to 40 GPa, with an analysis of anisotropy and mechanical properties indicating a ductile nature. The electronic structure, dominated by Mo-*d* and N-*p* states, suggests potential applications in electronic systems, with features such as a high density of states at the Fermi level pointing to superconductivity. Thermodynamic properties, including heat capacities, Debye temperature, and entropy, are evaluated under varying temperatures and pressures, demonstrating its thermal stability and suitability for high-performance applications. These results provide a comprehensive understanding of the $LiMoN_2$ compound's properties and its potential for advanced material applications.

Keywords: $LiMoN_2$ compound, ab initio calculations, density functional theory (DFT), and hexagonal structure

DOI: 10.1134/S1063783425600499

1. INTRODUCTION

Layered and quaternary nitrides, such as $LiMoN_2$, $LiSrGaN_2$, $LiCrS_2$, and $LiVS_2$, exhibit intriguing chemical, magnetic, electronic, and thermodynamic properties that make them potential candidates for applications in energy storage, catalysis, and magnetic devices. $LiMoN_2$, synthesized via ammonolysis of molecular precursors or ternary oxides at 650–710°C, is the first metallic layered nitride capable of lithium deintercalation and reintercalation, although limited by significant hysteresis during electrochemical cycling. It exhibits Pauli paramagnetism and metallic conductivity due to strong electronic interactions within MoN_2 layers, despite the presence of anti-site defects (~15%) that modify its structural and electronic behavior [1]. Similarly, $LiSrGaN_2$, synthesized under oxygen-free conditions using molten sodium, features interpenetrating two-dimensional $[GaN_4]^{5-}$ and $[LiN]^{4-}$ networks that resemble layered silicates, offering structural stability and potential catalytic

applications [2]. In contrast, $LiCrS_2$ and $LiVS_2$, derived from reactions between lithium carbonate and metal oxides under H_2S gas, adopt a hexagonal NiAs-type structure. $LiCrS_2$ exhibits antiferromagnetic ordering below 55 K, with a "third-type" triangular spin arrangement in hexagonal planes, while $LiVS_2$ lacks magnetic ordering, reflecting the sensitivity of magnetic properties to atomic composition [3]. Thermodynamically, $LiMoN_2$ faces challenges due to interlayer interactions, making lithium removal incomplete, whereas TiN_2 and $LiSrGaN_2$ display greater stability due to their negative formation energies and robust structural motifs [2, 4]. These materials' unique layered architectures, metallic and magnetic properties, and structural tunability position them as promising candidates for advanced energy and electronic systems. This compound is a member of a family of layered nitrides that includes $LiWN_2$ and sulfides $LiVS_2$, and $LiSrGaN_2$ as quaternary nitrides [5]. The three studies collectively provide an integrated analysis of ternary nitride compounds, including $MgMoN_2$, Ca_4TiN_4, and molybdenum-based nitrides such as Fe_3Mo_3N and Co_3Mo_3N. The first study focused on the feasibility of magnesium extraction and reinsertion in $MgMoN_2$. Experimental and theoretical results revealed high energy barriers (~1.8 eV) for Mg^{2+} ion migration, rendering the compound unsuitable for current electrochemical applications. However, the study offers valuable insights for designing future cathodes [6–8]. The second study investigated the structural, electronic, and thermodynamic properties of Ca_4TiN_4 using ab initio simulations. The compound exhibited an indirect band gap (1.625 eV), mechanical stability, and unique chemical bonding combining ionic and covalent characteristics, making it a promising candidate for optical and mechanical applications [9, 10]. Lastly, the third study examined the synthesis and characterization of ternary molybdenum nitrides, such as Fe_3Mo_3N and Co_3Mo_3N, which demonstrated high stability under oxidative conditions and distinctive metallic behavior, highlighting their potential in catalytic and technological applications [11, 12]. Together, these studies represent significant advancements in understanding and designing nitride-based materials for diverse applications.

The objective of this research is to investigate the structural, elastic, mechanical, electronic, and thermodynamic properties of the $LiMoN_2$ compound using ab initio calculations based on density functional theory (DFT). The study intends to comprehend its metallic nature and possible superconducting capabilities by examining its stability, mechanical behavior, and electrical structure. Its applicability for high-performance applications is further evaluated by thermodynamic analyses conducted at different pressures and temperatures. These discoveries offer a thorough comprehension of $LiMoN_2$ and aid in the creation of cutting-edge materials for energy storage and technological devices.

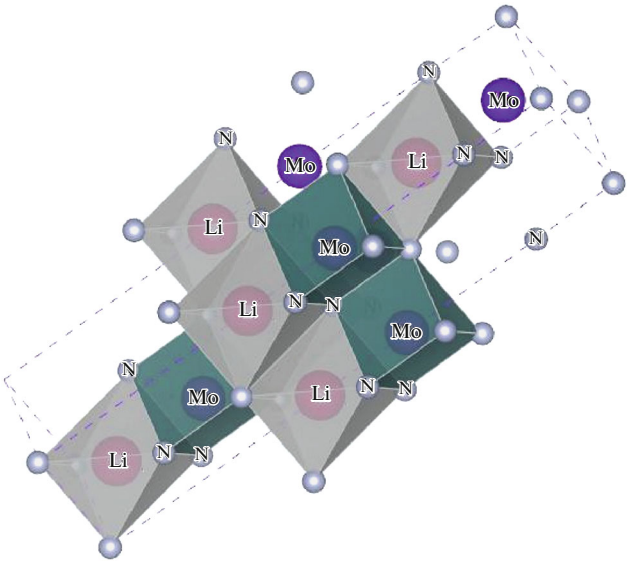

Fig. 1. Unit-cell of hexagonal crystal structure of $LiMoN_2$ in conventional cell.

2. COMPUTATIONAL METHOD

$LiMoN_2$ compound has the tetragonal structure $R3$ (146), $Z = 3$, $a = b = 2.8674(3)$ Å, $c = 15.801(2)$ Å presented in Fig. 1. Based on the formalism of the density functional theory (DFT) [12, 13], the theoretical calculations were carried out using the CASTEP simulation program (Cambridge Serial Total Energy Package) [14]. it is the generalized gradient approximation GGA that we used to determine the exchange and correlation potential, that is parameterized by Perdew, Burke, Ernzerhof (1996) [15], We define a starting density, to determine the potential and the resolution of the Schrödinger equation which gives the eigenfunctions and the eigenvalues. The cycle repeats until convergence is reached. In addition, a new density is generated by the calculated eigenfunctions. The norm conserving potential were used to describe only the valence electrons in the calculations, in which Li($1s^2\ 2s^1$), Mo($4s^2\ 4p^6\ 4d^5\ 5s^1$) and N($2s^2\ 2p^3$) orbitals are treated as valence electrons. High Kutoff energy of 560 eV is used even though we spend a lot of time getting good results. To sample the Brillouin zone, we use the Monkhorst–Packet 6 × 6 × 6 [16]. To determine the equilibrium network parameter we optimize the structure, so we used the Broyden–Fletcher–Goldfarb–Shenno (BFGS) minimization technique. For a complete optimization, BFGS makes it possible to find the structure at low energy, with the thresholds of the internal constraints and the forces exerted on each atom which are negligible, (i) energy change per atom less than 2×10^{-5} eV, (ii) residual force less than

0.05 eV/Å, (iii) atom displacement during geometry optimization less than 0.002 Å and (iv) maximum stress within 0.1 GPa.

3. RESULTS AND DISCUSSION

3.1. Structural Properties

The structure of $LiMoN_2$ is shown in Fig. 1 and its conception may be as being composed of layers of MoN_2 intercalated by Li. The additional electron of the Li atom leads to a compound with a metallic character. The nitrogen coordination in $LiMoN_2$ compound places the molybdenum in this space groups $R3$ in a trigonal prismatic hole. The assumed atomic positions in this space group are listed in Table 1.

We must first investigate and examine the convergence of calculated total energies with respect to the plane wave cut-off Ecut in the hexagonal solid phase of the $LiMoN_2$ compound Fig. 1. The number of points can be arbitrarily increased to increase the precision of calculations but these increase the computational cost [18]. Secondly, we examine the convergence of calculated number of points of our computed compounds that are 6 × 6 × 6 of c-Fe_2Hf and h-Fe_2Hf.

We must first investigate the energy cutoff without taking account the spin polarized, and examine the convergence of calculated total energies with respect to the plane wave cut-off E_{cut} in the hexagonal solid phases of the molecular system to be 560 eV for $LiMoN_2$ (Fig. 2a). The total energy as a function of the number of k points is shown in Fig. 2b. The convergence was obtained in sampling k points of 1 × 1 × 1 for a total energy convergence tolerance (1.0×10^{-6} eV/atom). The calculated number of points of our computed compounds $LiMoN_2$ are 6 × 6 × 6.

Table 1. Ideal positional parameters initially proposed for the possible structure of $LiMoN_2$. Space group $R3$ (no. 146). Cell parameters (Å) for the X-ray case: a = 2.8674(3), c = 15.801(2) [17]

Atoms	Site	x/a	y/b	z/c
Mo	3a	0(0)	0(0)	0(0)
Li	3a	0(0)	0(0)	0.827(0.833)
N(1)	3a	0(0)	0(0)	0.25(0.25)
N(2)	3a	0(0)	0(0)	0.41(0.41)

In parentheses the experimental values.

During compression, a decrease in volume increases the internal pressure of a system, the opposite is true during expansion, an increase in volume decreases the internal pressure, and whether in a compression or a relaxation, the energy variation with respect to volume or nearest neighbor distance is considered an important test of validity for interatomic potentials. In Fig. 3, We apply the density functional, we show the plot of energy, volume and the c/a ratio versus pressures of $LiMoN_2$ in hexagonal structures up to 40 GPa. Where the energy (a) passes through a minimum marking the state of physical equilibrium, in

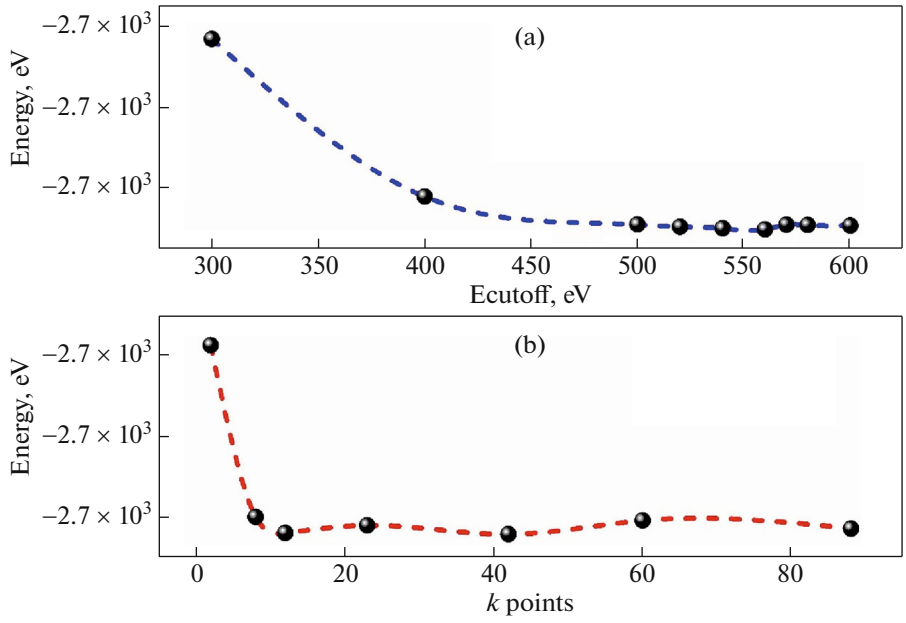

Fig. 2. Shows a plot of the energy against the energy cutoff (a) and the number of k points (b) in the hexagonal crystal structure of our calculated compound.

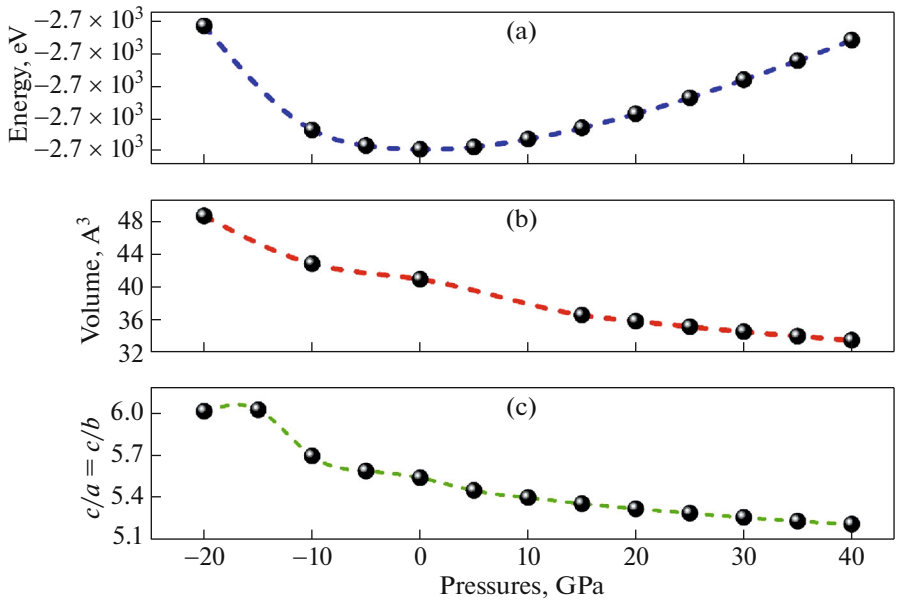

Fig. 3. Energy (a), volume (b), and c/a (c) versus pressures of $LiMoN_2$ in hexagonal structure.

(b) and (c) the curves decrease linearly. The calculated cell parameters are presented in Table 2.

3.2. Elastic Properties

By means of a Taylor series expansion of the total energy, $E(V, \delta)$, the elastic constants are defined for the system compared to a small deformation δ of the lattice unit cell volume V. The energy of system constraint is expressed as follows [20]

$$E(V,\delta) = E(V_0,0) + V_0\left[\sum_i \tau_i\xi_i\delta_i + \frac{1}{2}\sum_{ij} C_{ij}\delta_i\xi_i\delta_j\right], \quad (1)$$

where $E(V_0, 0)$ is the energy of the unstrained system with equilibrium volume V_0, τ_i is an element in the stress tensor, and ξ_i is a factor to take care of Voigt index. Between 21 and 2 independent elastic constants, the number of independent elastic constants is 5 for hexagonal crystals which correspond to an asymmetric and isotropic material, called C_{11}, C_{33}, C_{44}, C_{12}, and C_{13}. The calculation of the elastic constants of solids provides information on the stability and rigidity of materials, on the nature of the forces acting in solids and establishes a link between the mechanical and dynamic behaviors of crystals.

Table 2. Cell parameters

$LiMoN_2$	Experiment [10]	LDA/CA-PZ	GGA/PBE
Space group	*R*3 (N°146)	*R*3 (N°146)	*R*3 (N°146)
Lattice parameter: *a* (Å)	2.8674(3)	2.867	2.958616
b (Å)	2.8674(3)	2.867	2.958616
c (Å)	15.801(2)	15.848	16.035983
c/*a*	5.5105	5.527	5.420
c/*b*	5.5105	5.527	5.420
Cell volume (Å^3)	112.479	112.816	121.563
Z	3	3	3
Calculated density (g cm^{-3})	5.79722	5.77987	5.363976
Number of atoms in cell	12	12	12
Final energy, eV	–	−2303.93	−2303.83

Note that the calculated values are in a good agreement with those observed experimentally by Yvon et al. (in parentheses) [19].

Since the derivatives of the first and second order potential give forces and elastic constants. It is therefore important to check the accuracy of the calculations of forces and elastic constants. The effect of pressure on elastic constants is essential especially for phase transition mechanisms, or to understand interatomic interactions and the mechanical stability of materials. The corresponding bulk moduli are determined as a function of pressure up to 40 GPa for hexagonal $LiMoN_2$ structures. Let us notice that all elastic constants as well as both bulk moduli linearly increase when pressure is enhanced.

For $LiMoN_2$ in a hexagonal crystal, let us recall that the generalized elastic stability criteria [21] are:

$$C_{11} > 0, \quad C_{33} > 0, \quad C_{44} > 0, \quad C_{66} > 0,$$
$$C_{11} - C_{12} > 0, \quad C_{11} + C_{33} + C_{12} > 0, \qquad (2)$$
$$(C_{11} + C_{12})C_{33} - 2C_{13}^2 > 0.$$

For $LiMoN_2$ with hexagonal structure, the shear anisotropy factor $A(C_{ij})$, defined as $A = 4C_{44}/(C_{11} + C_{33} - 2C_{13})$ for the {100} shear planes between the ⟨011⟩ and ⟨010⟩ directions, [22] as well as the ratio between linear compressibility coefficients for hexagonal crystals, i.e., $k_c/k_a = (C_{11} + C_{12} - 2C_{13})/(C_{33} - C_{13})$. The computed shear anisotropic factors are listed in Table 3.

For hexagonal structures, bulk modulus B, shear modulus G are obtained as follows:

$$B = \frac{2}{9}\left(C_{11} + C_{12} + 2C_{13} + \frac{1}{2}C_{33}\right), \qquad (3)$$

$$G = \left\{C_{44}\left[\frac{C_{44}(C_{11} - C_{12})}{2}\right]^{1/2}\right\}^{1/2}. \qquad (4)$$

In addition, Young's modulus E can be obtained according to Cline et al. [23]:

$$E = \frac{\left[C_{33}(C_{11} + C_{12}) - 2C_{13}^2\right](C_{11} - C_{12})}{C_{11}C_{33} - C_{13}^2}, \qquad (5)$$

whereas anisotropy value A and Poisson's ratio are expressed as:

$$A = \frac{2C_{44}}{C_{11} - C_{12}}, \qquad (6)$$

$$\nu = \frac{C_{12}C_{33} - C_{13}^2}{C_{11}C_{33} - C_{13}^2}. \qquad (7)$$

To quantify whether a material would break in a ductile or brittle manner Pugh [24], proposed the ratio between the bulk modulus and the shear modulus (B/G) of polycrystalline phases. Subsequently, a high value of this ratio is associated with ductility and vice versa. The critical value, which separates the ductile character from the fragile one, is 1.75.

Table 3. Calculated bulk modulus, elastic constants, shear modulus G, Young's modulus Y and Poisson's ratio ν for $LiMoN_2$ structure at $P = 0$ GPa in Reuss approximation, all constants are in GPa except ν dimensionless

Parameters	$LiMoN_2$-GGA/PBE	$LiMoN_2$-LDA/CA-PZ
B (GPa)	148.18	168.99
C_{11}	422.8	475.23
C_{12}	137.93	174.15
C_{13}	46.2	52.38
C_{33}	226.8	256.32
C_{44}	14.8	34.35
C_{14}	1.34	−3.342
C_{15}	0.1089	−0.0146
Y	89.219	168.86
ν	0.399	0.33
G	31.87	63.31

For instance, diamond has a B/G of 0.80 [25], while aluminum, cobalt, rhodium and iridium present B/G ratios of 3.04, 2.4, 1.83, and 1.52, respectively.

From our B/G calculated ratios for the hexagonal $LiMoN_2$ compounds, we obtain www, xxx, and ccc, respectively. The fact that $LiMoN_2$ compounds are ductile compounds. Additionally, the mechanical stability of the hexagonal structure at 0 GPa can be predicted from the elastic constants data ($C_{11} - C_{12} > 0$). To be complete, the elastic constants of pure $LiMoN_2$ in hexagonal structures are listed in Table 3.

The Debye temperature may be estimated from the average sound velocity V_m [26, 27]

$$\Theta = \frac{h}{k}\left[\frac{3n}{4\pi}\left(\frac{N_A\rho}{M}\right)\right]^{1/3} V_m, \qquad (8)$$

where h is Planck's constants, k is Boltzman's constant, N_A is Avogadro's number, n is the number of atoms per formula unit, M is the molecular mass per formula unit, ρ is the density, and V_m is obtained from [28]

$$V_m = \left[\frac{1}{3}\left(\frac{2}{V_s^3} + \frac{1}{V_l^3}\right)\right]^{-1/3}, \qquad (9)$$

where V_s and V_l are the shear and longitudinal sound velocities, respectively.

The arithmetic average of the Voigt and the Reuss bounds is called the Voigt–Reuss–Hill (VRH) average and is commonly used to estimate elastic moduli

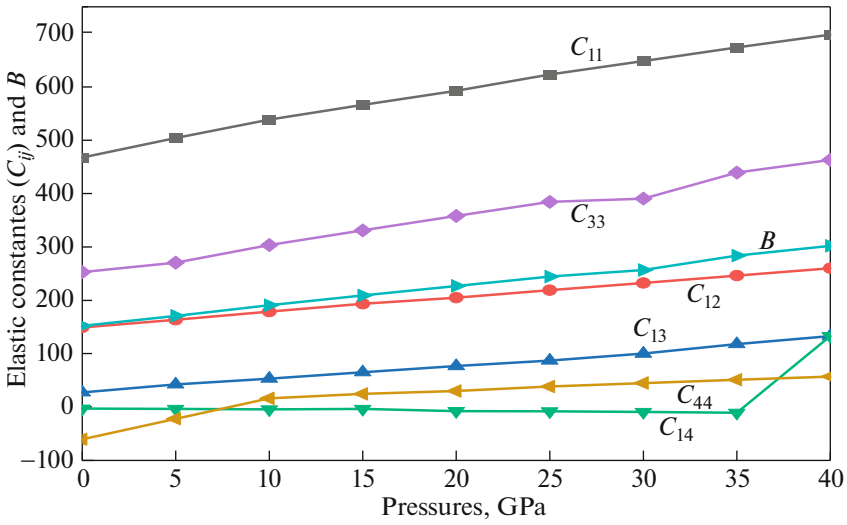

Fig. 4. The elastic constants of the hexagonal structure of $LiMoN_2$ compound under pressure up to 40 GPa at 0 K (LDA/CA-PZ).

of polycrystals. The VRH averages for shear modulus (G) and bulk modulus (B) are

$$G = \frac{1}{2}(G_R + G_V), \quad B = \frac{1}{2}(B_R + B_V). \tag{10}$$

The polycrystalline moduli are the arithmetic mean values of the Voigt and Reuss moduli [29]:

$$G_H = \frac{1}{2}(G_R + G_V), \quad B_H = \frac{1}{2}(B_R + B_V). \tag{11}$$

Therefore, the probable values of the average shear and longitudinal sound velocities can be calculated from Navier's equation [30]:

$$V_S = \sqrt{\frac{G_H}{\rho}}, \quad V_L = \sqrt{\frac{\left(B_H + \frac{4}{3}G_H\right)}{\rho}}. \tag{12}$$

The longitudinal, transverse and average sound velocities and Debye temperature of cubic and hexagonal of $LiMoN_2$ in hexagonal structures have been calculated and listed in Table 3.

At zero pressure and zero temperature, we have calculated the sound velocities and Debye temperature for the $LiMoN_2$ compounds from our elastic constants. Our calculated sound velocities and Debye temperature are comparable to the experimental values.

The elastic constants of the hexagonal structure of the $LiMoN_2$ compound under pressures up to 40 GPa at 0 K (Fig. 4**)**, calculated using the LDA/CA-PZ method. These constants (C_{11}, C_{12}, C_{33}, C_{44}, etc.) quantify the mechanical response and structural stability under applied stress. Conducted at 0 K, the simulations rely on density functional theory (DFT) within the local density approximation (LDA). The variation of elastic constants with pressure offers insights into potential phase transitions or structural changes, while adherence to mechanical stability criteria under pressure validates the compound's robustness. These results are crucial for understanding the material's behavior under extreme conditions.

3.3. Anisotropic Index and Elastic Debye Temperature

The anisotropic index and elastic Debye temperature of the hexagonal structure of the $LiMoN_2$ compound under pressure at 0 K (Fig. 5). The anisotropic index highlights the directional dependence of the material's elastic properties, reflecting variations in its mechanical response along different crystallographic axes. The elastic Debye temperature, related to the average sound velocity, provides insights into the lattice vibrations and thermal properties of the compound. These parameters, analyzed under high pressure and at 0 K, are crucial for evaluating the mechanical anisotropy and thermodynamic stability of the material in extreme conditions.

3.4. Electronic Structure

The document presents the electronic band structure of the hexagonal $LiMoN_2$ compound**.** This provides critical insights into the electronic properties, including the energy distribution of electrons and the potential presence of a bandgap. The analysis is key to understanding the material's electrical conductivity, optical properties, and potential applications in electronic or optoelectronic devices. The electronic bandstructure of $LiMoN_2$ is depicted in Fig. 6, together

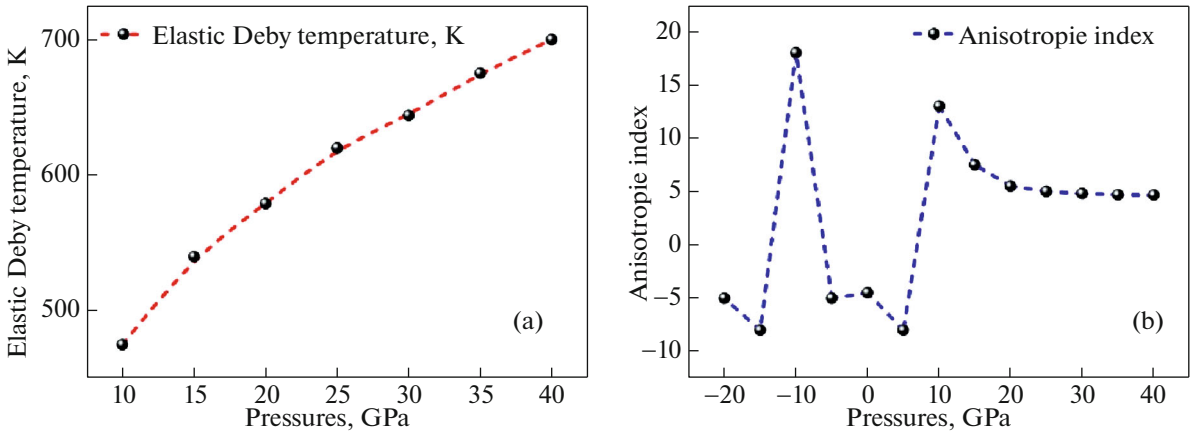

Fig. 5. The anisotropic index (a) and elastic Debye temperature (b) of the hexagonal structure of $LiMoN_2$ compound under pressure at 0 K.

with the atom resolved and total density of electronic states Fig. 7. The total DOS reveals the overall distribution of electronic states across energy levels, while the partial DOS breaks this down by contributions from specific atomic orbitals. This analysis is fundamental for understanding the electronic structure, including the role of individual elements and orbitals in the material's bonding, conductivity, and potential electronic applications.

We keep the description of the electronic properties of $LiMoN_2$. We show here only the vicinity of the Fermi energy level. There are two bands crossing the Fermi level which are composed of *d*-Mo states strongly hybridized with *p*-N states. We see almost no contribution from Li to the density of states, indicating that these atoms are fully ionized. Finally, the Fermi level is located on a very large peak in density of states, a fact often associated with superconductivity and play a dominant role in electrical transport. If we look at the total density of states (DOS) lion from the Femi level and in the valence band we observe that there are two broad peaks, the bond decomposition indicates

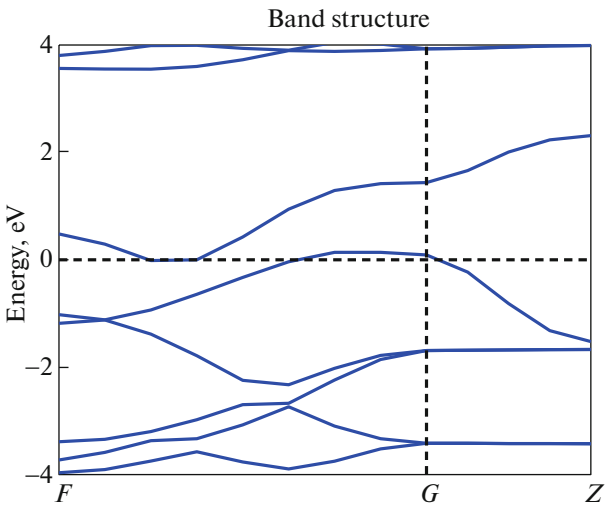

Fig. 6. The electronic band of the hexagonal structure of $LiMoN_2$ compound.

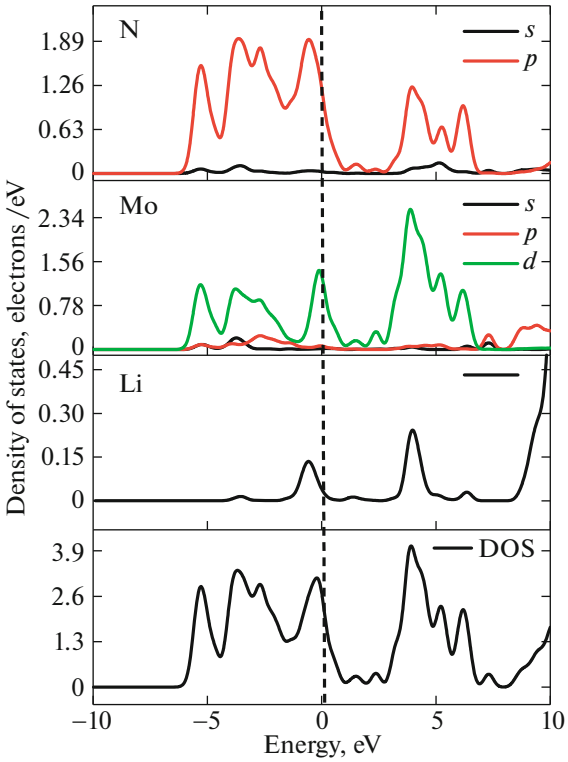

Fig. 7. The total and partial electronic densities of states of $LiMoN_2$ in hexagonal structure without spin polarized.

Table 4. Atomic populations (Mulliken) of all electron configurations of $LiMoN_2$ atoms

Species	*s*-Orbitals	*p*-Orbitals	*d*-Orbitals	Total	Charge (e)
Li	−0.43	0.50	0	0.07	0.87
N	0.89	1.94	0	2.83	−0.65
N	0.89	1.96	0	2.85	−0.70
Mo	0.33	0.04	2.39	2.76	0.48

that the structure between −6 and 0 eV has a mixed character of *d*-Mo, *p*-N and a weak contribution of *s*-Li especially when approaching the Fermi level. In the conduction band, there are the same contributions especially between 3 and 8 eV. The strong contribution of *s*-Li states only appears at high energies.

3.5. Population Analysis

The Mulliken population of chemically linked atom pairs indicates the concentration of electronic charge in the bonding region. Its value is often proportional to the strength of the bonds between atoms. She may be interested in the valence state of an atom in a molecule and the chemical bonds between individual atoms. A negative overlap population between chemically unbonded atoms suggests an anti-bonding and repulsive interaction. We undertake the population analysis using Mulliken's formalism [31]. According to [32], analyzing Mulliken populations can yield valuable insights. Atomic populations (Mulliken) of all electron configurations of $LiMoN_2$ atoms arise from Mulliken population analysis and provide a means of estimating partial atomic charges, particularly those based on the linear combination of atomic orbitals see Table 4. Our compound is not very large molecule so we also intended to compare experimental results (from X-ray crystallography) with theoretically calculated properties at the highest level that was available. Table 5 reports some interatomic distances of interest and presents a comparison of those obtained experimentally [1] and calculated by ab initio method.

Table 5. Ab initio values for the bond lengths and angles of $LiMoN_2$ compound

Bond	Length, Å
Mo_1–$N_{1\times3}$	2.104 (2.095)
Mo_1–$N_{2\times3}$	2.143 (2.091)
Li_1–$N_{1\times3}$	2.257 (2.179)
Li_1–$N_{2\times3}$	2.139 (2.098)
Angle	**Values, deg**
N_1–Mo_1–$N_{1\times6}$	88.61 (86.34)
N_1–Mo_1–$N_{2\times3}$	72.81 (75.45)
N_1–Mo_1–$N_{2\times6}$	132.54 (133.41)
N_1–Li_1–$N_{1\times3}$	81.27 (82.38)
N_1–Li_1–$N_{2\times6}$	94.27 (95.72)
N_1–Li_1–$N_{2\times3}$	178.99 (177.39)
N_2–Li_1–$N_{2\times3}$	89.15 (86.29)

The resulting average Li1–N1 (Mo1–N2) bond length for $LiMoN_2$ of 2.257 (2.143) Å, is just slightly longer than the Li1–N2 (Mo1–N1) of 2.139 (2.104) Å (see Table 5). Note here that the ab initio values for the bond lengths and angles are much closer with the experimental ones. Another interesting observation concerns the almost linear (perpendicular) arrangement of atoms N1–Li1–N2×3 with angles of 178.99° (N1–Li1–N2×6 with angle 94.27) and less for N1–Mo1–N2×6 with angles of 132.54° (N1–Mo1–N2×3 with angles of 72.81°).

3.6. Thermodynamic Properties

Thermodynamics is the dependence of the physical properties of bodies on temperature, which becomes more important over the years, thermal exchanges and transformations occur. Thermodynamics focuses on analyzing the structure of matter and establishing a link between its properties.

Transformations can have different characteristics: at constant pressure, at constant volume and at constant temperature. Engines with very high operating temperatures will require materials or melting temperatures are very high for these applications, a chemical and crystalline study must be carried out.

In our study we focus on the behavior of some physical constants, such as the specific heat at constant volume, the specific heat at constant pressure, the entropy, the compressibility modulus, the Debye temperature as a function of temperature (between 0 and 600 K) at constant pressure and as a function of the pressure 0, 2, 4, 6, 8, 10 GPa at constant temperatures. C_v, C_p, S and alpha are the most important characteristics, C_v, C_p, S and alpha as a function of temperatures (at constant pressure $P = 0, 2, 4, ..., 10$ GPa

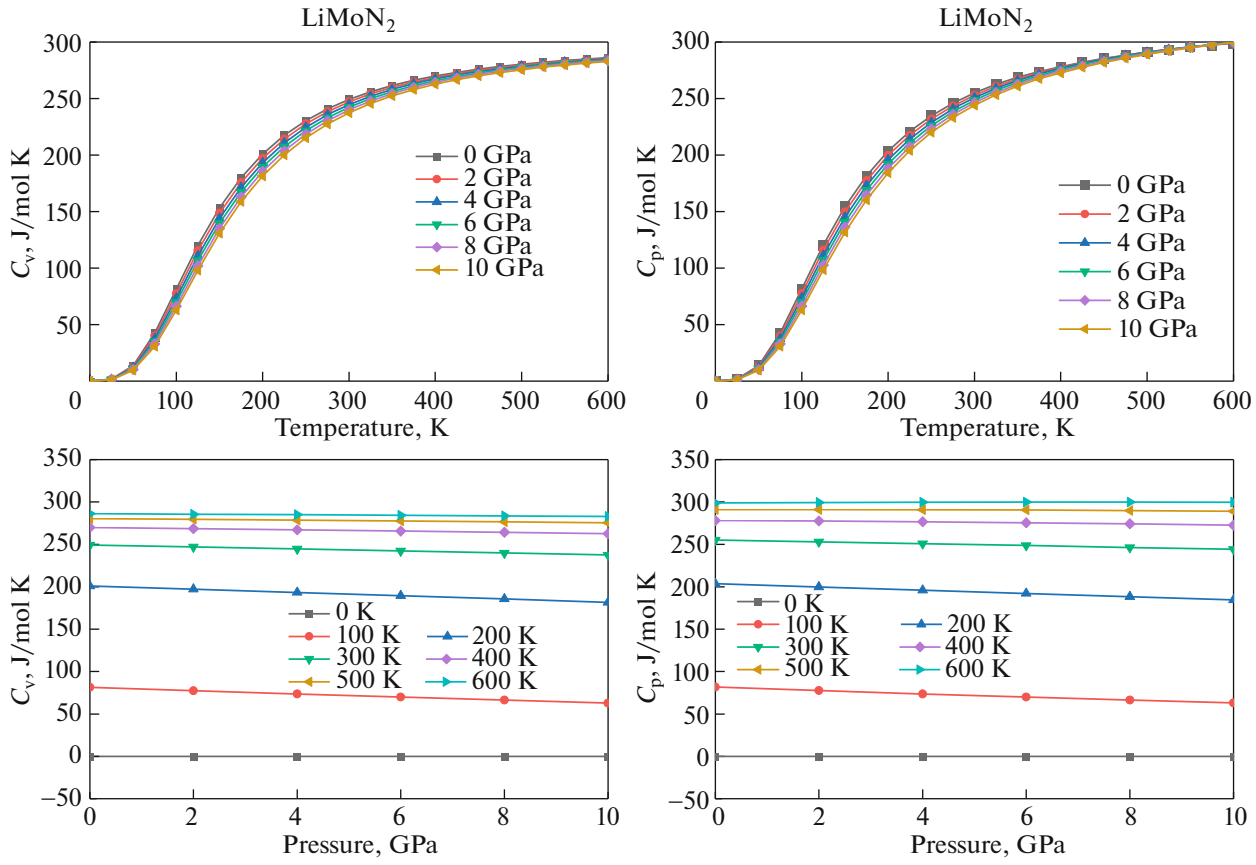

Fig. 8. The heat capacities at constant volume (C_v) and constant pressure (C_p) versus temperature and pressure of $LiMoN_2$ compound.

have the same appearance and are almost parabolic function and varies little depending on the pressure), and of pressures (at constant temperatures $T = 0$, 100, 200, ..., 600 K, they are linear variation, meaning that the quantity of heat that this material is constant at the pressure).

B decreases slightly (at constant pressure) when the temperature increases and increases linearly (at constant temperature) when the pressure increases. The thermodynamic properties of the $LiMoN_2$ compound are studied under varying temperatures and pressures. Figure 8 compares the heat capacities at constant volume (C_v) and constant pressure (C_p), providing a comprehensive understanding of the compound's thermal behavior. These analyses are crucial for evaluating $LiMoN_2$'s performance in high-temperature and high-pressure environments. highlights the heat capacity at constant volume (C_v), showing the material's ability to store thermal energy. Figure 9 presents the Debye temperature (θ_D), reflecting lattice vibrations, and the bulk modulus (*B*), indicating resistance to compression, Debye temperature θ_D at constant pressure and low temperature is almost constant, and it gradually decreases with temperature. Debye temperature increases with constant pressure and temperature.

4. CONCLUSIONS

The $LiMoN_2$ compound's exceptional structural, mechanical, electrical, and thermodynamic capabilities have been uncovered by a thorough ab initio investigation. The hexagonal structure, with strong Mo–N bonding, exhibits mechanical stability and a ductile nature. Elastic constants and anisotropy factors validate its robustness under high pressures. The electronic structure, characterized by significant Mo-*d* and N-*p* state contributions, confirms its metallic conductivity and potential for superconducting applications. Furthermore, the compound demonstrates thermal stability under various conditions, with heat capacities, Debye temperature, and entropy showing consistent trends. These findings establish $LiMoN_2$ as a promising material for energy, electronic, and high-temperature applications. In order to better evaluate its technical uses, future research might investigate its potential in dynamic situations, such as electrochemical cycling.

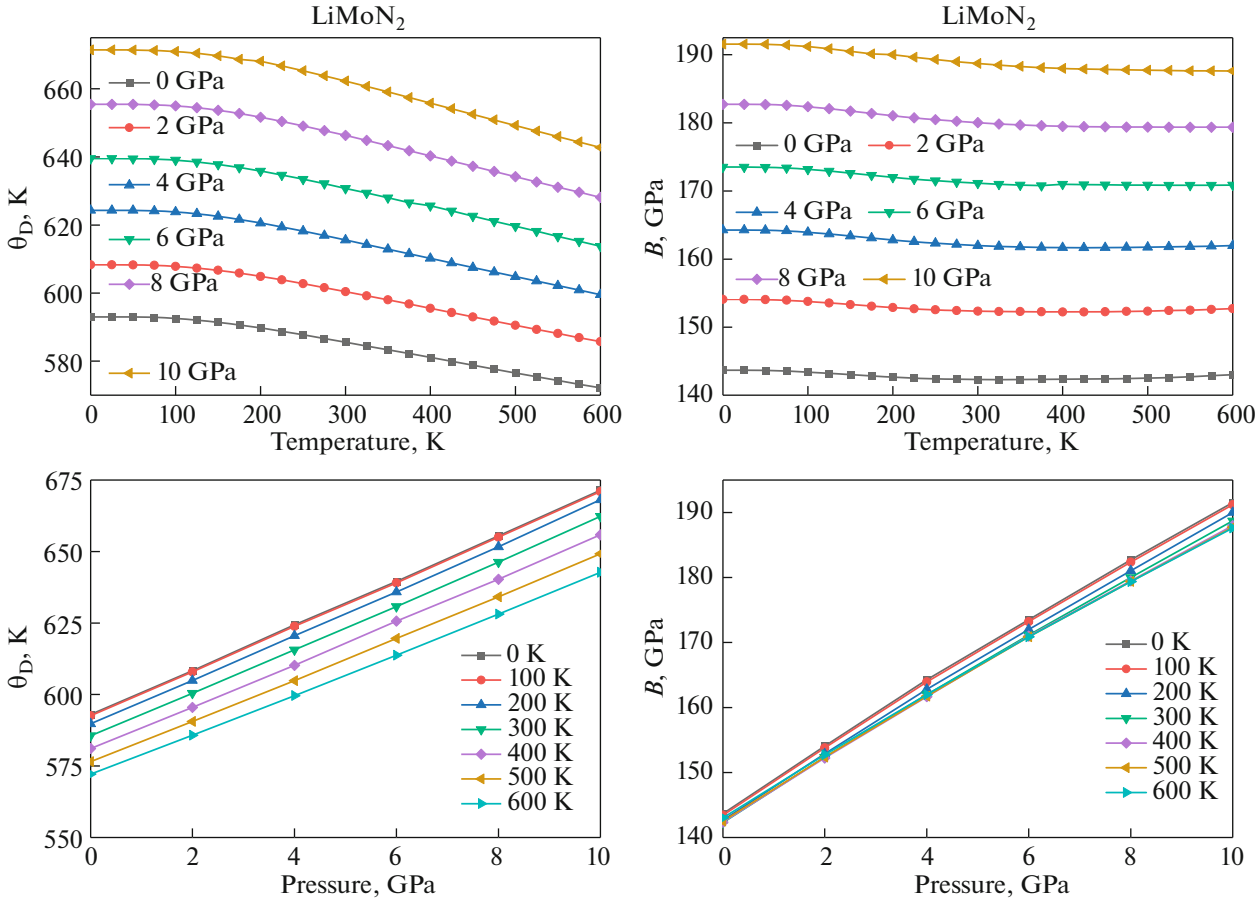

Fig. 9. The Debye temperature θ_D and bulk modulus B versus temperature and pressure of $LiMoN_2$ compound.

AUTHOR CONTRIBUTION

Conceptualization: A. Djemli, Z. Zerrougui.

Data curation: F. Benlakhdar, M. Reffas.

Formal analysis: K. Bouferrache, B. Ghebouli.

Methodology: M.A. Ghebouli, R. Yekhlef, D. Belfennache.

Writing and review and editing: T. Chihi.

Validation: M. Fatmi, Sameh I. Ahmed.

FUNDING

This research was funded by Taif University, Saudi Arabia, Project no. TU-DSPP-2024-281.

DATA AVAILABILITY

Data underlying the results presented in this paper are not publicly available at this time but may be obtained from the corresponding author (fatmimessaoud@yahoo.fr) upon reasonable request.

CONFLICT OF INTEREST

The authors of this work declare that they have no conflicts of interest.

REFERENCES

1. S. Elder, L. H. Doerrer, F. DiSalvo, J. Parise, D. Guyomard, and J. Tarascon, Chem. Mater. **4**, 928 (1992).
2. D. G. Park, Z. A. Gál, and F. J. DiSalvo, J. Alloys Compd. **353**, 107 (2003).
3. B. van Laar and D. J. W. Ijdo, J. Solid State Chem. **3**, 590 (1971).
4. B. Ozdemir, Comput. Condens. Matter **16**, e00335 (2018).
5. X. Zhou, Y. Liang, C. Gu, L. Fang, B. Chen, Y. Zhao, and S. Wang, Chem. Mater. **36** (17), 8514 (2024).
6. S. Alconchel, F. Sapina, D. Beltra, and A. Beltra, J. Mater. Chem. **8** (8), 1901 (1998).
7. J. D. Houmes, D. S. Bem, and H.-C. zur Loye, in *MRS Symposium Proceedings: Covalent Ceramics II: Non-Oxides*, Ed. by A. R. Barron, G. S. Fischman, M. A. Fury, A. F. Hepp (Materials Research Society, Boston, Mass., 1993), Vol. 327, p. 153.

8. *MRS Symposium Proceedings: Covalent Ceramics II: Non-Oxides*, Ed. by A. R. Barron, G. S. Fischman, M. A. Fury, and A. F. Hepp (Materials Research Society, Boston, Mass., 1993), Vol. 327.
9. D. S. Bem, C. P. Gibson, and H.-C. Zur, Chem. Mater. **5**, 397 (1993).
10. S. Boucenna, K. Haddadi, A. Bouhemadou, L. Louail, F. Soyalp, and R. Khenata, J. Mol. Graph. Modell. **92**, 74e85 (2019).
11. R. S. Ningthoujam and N. S. Gajbhiye, Prog. Mater. Sci. **70**, 50 (2015).
12. K. Bouferrache, M. A. Ghebouli, B. Ghebouli, M. Fatmi, H. Bouandas, T. Chihi, N. H. Alotaibi, S. Mohammad, M. Habila, and M. Sillanpää, Mater. Sci. Eng., B **308**, 117550 (2024).
13. K. Bouferrache, L. Krache, M.A. Ghebouli, B. Ghebouli, S. I. Ahmed, M. Fatmi, T. Chihi, and B. Gueridi, Chem. Phys. Impact **5**, 100110 (2024).
14. M. A. Ghebouli, B. Ghebouli, T. Chihi, and M. Fatmi, Phys. B: Condens. Matter **610**, 412858 (2021).
15. L. Krache, M. A. Ghebouli, B. Ghebouli, S. Alomairy, M. Reffas, M. Fatmi, and T. Chihi, Phys. Status Solidi B **259** (10), 2200042 (2022).
16. R. Boudissa, Z. Zerrougui, M. A. Ghebouli, K. Bouferrache, L. Krache, T. Chihi, B. Ghebouli, M. A. Habila, M. Fatmi, and M. Sillanpää, Biophys. Rep. **37**, 101601 (2024).
17. R. Verrelli, A. P. Black, C. Frontera, J. Oró-Solé, M. E. Arroyo-de Dompablo, A. Fuertes, and M. R. Palacín, ACS Omega **4** (5), 8943 (2019).
18. F. Weber, L. Pintschovius, W. Reichardt, R. Heid, K.-P. Bohnen, A. Kreyssig, D. Reznik, and K. Hradil, Phys. Rev. B **89**, 104503 (2014).
19. K. Yvon, W. Jeitschko, and E. J. Parthe, Appl. Crystallogr. **10**, 73 (1977).
20. L. Fast, J. M. Wills, B. Johansson, and O. Eriksson, Phys. Rev. B **51**, 17431 (1995).
21. B. Ghebouli, M. A. Ghebouli, T. Chihi, M. Fatmi, S. Boucetta, and M. Reffas, Solid State Commun. **149** (47–48), 2244 (2009).
22. P. Ravindran, L. Fast, P. A. Korzhavyi, B. Johansson, J. Wills, and O. Eriksson, J. Appl. Phys. **84**, 4891 (1998).
23. C. F. Cline, H. L. Dunegan, and G. W. Henderson, J. Appl. Phys. **38**, 1944 (1967).
24. S. F. Pugh, Philos. Mag. **45**, 823 (1954).
25. J. Haines, J. M. Leger, and G. Bocquillon, Annu. Rev. Mater. Res. **31**, 1 (2001).
26. T. Chihi, M. A. Ghebouli, and M. Fatmi, Biochem. Biophys. Rep. **25**, 100923 (2021).
27. M. A. Ghebouli, T. Chihi, B. Ghebouli, and M. Fatmi, Chin. J. Phys. **56** (1), 323 (2018).
28. O. L. Anderson, J. Phys. Chem. Solids **24**, 909 (1963).
29. R. Hill, Proc. Soc. London A **65**, 350 (1952).
30. Z. Zerrougui, K. Bouferrache, M. A. Ghebouli, Y. Slimani, T. Chihi, B. Ghebouli, M. Fatmi, F. Benlakhdar, S. A. Mouhammad, N. Algethami, and S. Alomairy, Solid State Sci. **141**, 107211(2023).
31. R. S. Mulliken, J. Chem. Phys. **23**, 1833 (1955).
32. E. R. Davidson and S. Chakravorty, Theor. Chim. Acta **83**, 319 (1992).